

# Blue and Green-Mode Energy-Efficient Chemiresistive Sensor Array Realized by Rapid Ensemble Learning

Zeheng Wang <sup>1,2,†</sup>, James Cooper <sup>2</sup>, Muhammad Usman <sup>1,3</sup>, and Timothy van der Laan <sup>2</sup>

---

<sup>1</sup>Data61, CSIRO, Clayton, VIC 3168, Australia

<sup>2</sup>Manufacturing, CSIRO, West Lindfield, NSW 2070, Australia

<sup>3</sup>School of Physics, The University of Melbourne, Parkville, 3010, Victoria, Australia

† Corresponding author. Email: [zenwang@outlook.com](mailto:zenwang@outlook.com), [zeheng.wang@csiro.au](mailto:zeheng.wang@csiro.au)

---

Keywords: Chemiresistive sensor; Sensor array; Energy-efficient; Artificial intelligence; Ensemble learning.

## Abstract

The rapid advancement of Internet of Things (IoT) necessitates the development of optimized Chemiresistive Sensor (CRS) arrays that are both energy-efficient and capable. This study introduces a novel optimization strategy that employs a rapid ensemble learning-based model committee approach to achieve these goals. Utilizing machine learning models such as Elastic Net Regression, Random Forests, and XGBoost, among others, the strategy identifies the most impactful sensors in a CRS array for accurate classification: A weighted voting mechanism is introduced to aggregate the models' opinions in sensor selection, thereby setting up two distinct working modes, termed "Blue" and "Green". The Blue mode operates with all sensors for maximum detection capability, while the Green mode selectively activates only key sensors, significantly reducing energy consumption without compromising detection accuracy. The strategy is validated through theoretical calculations and Monte Carlo simulations, demonstrating its effectiveness and accuracy. The proposed optimization strategy not only elevates the detection capability of CRS arrays but also brings it closer to theoretical limits, promising significant implications for the development of low-cost, easily fabricable next-generation IoT sensor terminals.

## 1. Introduction

Chemiresistive sensors (CRSs) are increasingly recognized as pivotal components in the sensing network of the Internet of Things (IoT) [1], [2], [3], [4]. Their growing prominence is attributed to several key advantages, including straightforward manufacturing processes [5], a broad range of detectable analytes [6], and rapid readout [7], [8]. Over the years, comprehensive research has unequivocally demonstrated the versatility of chemiresistive sensors across a multitude of applications. These range from medical diagnostics, particularly in the realm of disease diagnosis [8], to environmental applications such as real-time air quality assessment [9] and the detection of various pollutants [10], [11].

Distinct from traditional analytical instruments, which often rely on complex and time-consuming procedures, CRSs operate on a more straightforward principle: the modulation of electrical resistance in the presence of target chemicals [12], [13]. This change in resistance serves as the primary sensing mechanism and is influenced by the type of material constituting the sensor. For instance, metal nanoparticle (MNP)-based sensors and inorganic semiconductor-based sensors each have unique mechanisms that govern their response to different analytes [12], [14]. Despite these variations, the core principle remains consistent—different analytes induce distinct changes in the sensor's conductivity. As a result, by quantitatively measuring these resistance fluctuations, one can directly infer the characteristics of the sample under investigation.

In practical scenarios, CRSs often face the challenging task of distinguishing between analytes that possess closely related physiochemical properties — a feat that is difficult to achieve with a single sensor. To address this limitation, sensor arrays or networks are employed [15], [16], [17]. Within such an array, each sensor exhibits a unique sensitivity to various analytes, a phenomenon commonly termed as 'partial selectivity.' Leveraging this partial selectivity, the CRS array can function synergistically as a principal component analyzer [17]. In this capacity, it can identify distinct principal components, which may represent specific chemicals or combinations thereof, simply by monitoring the resistance changes across components in the array. Importantly, this approach obviates the need for each individual sensor to exhibit high selectivity towards any specific analyte. Instead, the strength of the array lies in its collective chemical diversity, enabling it to respond to a broader range of analytes with cross-reactive characteristics [18].

However, the deployment of CRS arrays in modern Internet of Things (IoT) applications presents a significant challenge in terms of energy consumption, as they are inherently resistive. Resistive behavior is naturally energy-intensive necessitating a careful evaluation of each sensor's performance to eliminate redundancy within the array, thereby conserving energy. This task becomes increasingly complex as the size of the CRS array expands. While various innovative approaches have been proposed to address this issue, e.g., clustering algorithms [19], search algorithms [20], and genetic algorithms [21], these methods often yield sensor subsets optimized for specific analytes, rather than offering a universally applicable solution. In addition, it has been proved that a single algorithm is typically unsuitable for all circumstances [22]. Therefore, there remains a pressing need for a comprehensive strategy that can effectively utilize less sensors in the array without compromising identification performance across a broad range of analytes.

In this study, we introduce a novel strategy aimed at optimizing CRS arrays through the use of artificial intelligence (AI)-based ensemble learning techniques. Specifically, we employ a diverse set of eight machine learning algorithms to model the sensor array's behavior. From these, we carefully select the top-performing models to form a 'model committee.' This committee operate on a weighted voting mechanism to identify essential sensors while eliminating redundant ones, thereby enhancing the array's efficiency. Our approach enables the sensor array to operate in two distinct modes: the 'Blue mode,' which utilizes the full array for maximum sensitivity, and the 'Green mode,' which employs a subset of sensors to achieve

nearly the same level of sensitivity but with reduced energy consumption. This is important as it would allow the system to generally operate in green mode to conserve power before switching to blue mode when required. To validate the efficacy of our strategy, we use the data from experiments comprising of 17 sensors detecting a group of aromatic compounds in a water-based solution [11]. Remarkably, our approach was able to narrow down the active sensors to just 5 in Green mode, with only a 4% reduction in detection capability. We also established a theoretical model that affirms optimization is possible and outlines the theoretical boundary of the optimization. This outcome underscores the potential of our approach for more generalized applications demanding both energy efficiency and high sensitivity, including wearable electronics and smart homes.

## 2. Theory and Methods

### 2.1. Theory of Detection Capability of CRS Array

Before embarking on the practical optimization of the CRS array, it is imperative to establish its theoretical feasibility. While constructing a comprehensive model that captures the responses and structures across all possible CRS array configurations is a daunting task, certain assumptions simplify the problem. Specifically, if we assume that: 1) the sensors in the array operate independently, 2) their readings never reach saturation, and 3) there is no cross-reactivity among analytes on the sensor surface, thereby ensuring linear contributions to the sensor's resistance change, the challenge can be reformulated as an optimization problem within the framework of stochastic processes.

In this case, the CRS array's responses to a sample can be depicted by a matrix  $D$ , where the element  $S_{ij}$  represents the  $i$ -th sensor's sensitivity to the  $j$ -th analyte. Usually, a single sensor in the CRS array will not to sense all analytes in the sample effectively, therefore, the matrix  $D$  will be a sparse matrix, i.e., each line has many zeros indicating that certain sensors cannot respond to certain analytes, such as:

$$D_{n \times m} = \begin{pmatrix} S_{11} & 0 & \cdots & S_{1m} \\ 0 & S_{22} & \cdots & \vdots \\ \vdots & S_{ij} & \ddots & 0 \\ S_{n1} & \cdots & 0 & 0 \end{pmatrix}. \quad (1)$$

The sample containing a series of analytes can be expressed by another diagonal matrix  $X$ :

$$X_{m \times m} = \begin{pmatrix} A_{11} & 0 & \cdots & 0 \\ 0 & A_{22} & \cdots & \vdots \\ \vdots & 0 & \ddots & 0 \\ 0 & \cdots & 0 & A_{mm} \end{pmatrix}. \quad (2)$$

Therefore, the matrix of one measurement,  $M$ , can be achieved by using the sensor matrix to multiply the sample matrix, which reads:

$$M = DX = \begin{pmatrix} S_{11}A_{11} & 0 & \cdots & S_{1m}A_{mm} \\ 0 & S_{22}A_{22} & \cdots & \vdots \\ \vdots & 0 & \ddots & 0 \\ S_{n1}A_{11} & \cdots & 0 & 0 \end{pmatrix}_{n \times m} = \begin{pmatrix} R_1 \\ R_2 \\ \vdots \\ R_n \end{pmatrix}, \quad (3)$$

Where vector  $R_i$  is  $i$ -th sensor's readout. Note that the elements of  $R_i$  are not explicit in a single readout, as the readout can only produce a single value combining all responses. The tomography of the matrix  $M$  can be realized by, e.g., ML algorithms. A perfect measurement requires  $M$  to have:

$$\exists k \leq n: \forall j \in [1, m], \left( \sum_{i=1}^k R_i \right)_j \neq 0. \quad (4)$$

The detection capability of the  $i$ -th sensor is quantified by the proportion of non-zero elements in its  $i$ -th row. Consequently, the overall detection capability of the CRS array is represented by the proportion of non-zero elements in the vector  $\sum_{i=1}^n R_i$ . For a given analyte  $j$ , the sum of the sensors' responses  $(\sum_{i=1}^k R_i)_j$  must be non-zero for a single measurement.

However, it's important to note that the CRS array may not be fully responsive to all analytes. Some analytes may elicit indistinguishable or even undetectable responses. In such cases, the  $j$ -th position in the response vector will be zero, indicating either a lack of response to the  $j$ -th analyte or an inability to distinguish this response from those to other analytes.

We assume that each sensor's detection capability (how many analytes it can identify),  $C_i$ , follows the Gaussian distribution  $\mathcal{N}$ :

$$1 - \epsilon_i = C_i \sim \mathcal{N}(\mu, \sigma^2), \quad (5)$$

Where  $\epsilon$  is the tolerance of the detection capability, which represents the system error rate of one sensor. Then, considering the array's system error  $C(n)$  (the percentage of the analytes that the array cannot identify), the optimization problem is (the detailed derivation can be found in Supplementary Material):

$$\text{Minimize } E[n], \quad \text{s. t. } \left[ 1 - \left( 1 - \frac{\mu}{m} \right)^{E[n_{\min}]} \right]^m - C(n) = 0, \quad n \in \mathbb{N}, \quad \epsilon \in (0,1), \quad (6)$$

Note that the whole array's error is the function of the number of the sensor  $n$ ,  $C(n)$ . Therefore, with the Lagrange multiplier  $\lambda$ , we will have the Lagrange function:

$$\mathcal{L}(n, \lambda) = E[n] + \lambda \left( C(n) - \left( 1 - \left( 1 - \frac{\mu}{m} \right)^n \right)^m \right). \quad (7)$$

We can then yield the optimization boundaries of the sensor number of the CRS array (the detailed derivation can be found in Supplementary Material):

$$E[n]_{min} = n \geq \frac{\ln(1 - \sqrt[m]{C})}{\ln(1 - \frac{\mu}{m})}. \quad (8)$$

Given the number of analytes in the sample, denoted as  $m$ , and the average detection capability of the CRS array, represented by  $\mu$ , we can establish a relationship between the minimum required number of sensors,  $n$ , and the constant system's detection capability,  $C$ . This demonstrates the feasibility of optimizing the CRS array. However, this theoretical framework only specifies the minimum number of sensors needed for effective measurement in Green mode; it does not address which specific sensors should be active. To tackle this remaining question, we will employ our proposed optimization strategy on a CRS array for detecting aromatic compounds in water. Subsequently, we will validate the practical outcomes against the theoretical predictions outlined in Eq. 8.

## 2.2. Optimization Strategy

The No Free Lunch Theorem in AI research posits that no single AI algorithm can serve as a one-size-fits-all solution for every problem, as evidenced by multiple studies [22], [23]. This theorem is particularly relevant when dealing with sensor arrays, which often exhibit diverse structures and behaviors, necessitating the consideration of multiple algorithms for effective optimization [24], [25]. Ensemble learning techniques offer a promising avenue to address this issue, where one single algorithm only partially affects the final decision, and the decision will be made by all eligible algorithms together. These techniques have been extensively researched and are known for their ability to mitigate the limitations imposed by the No Free Lunch Theorem to some extent [26], [27]. In light of this, our work leverages the concept of ensemble learning by incorporating a variety of AI models based on different algorithms to tackle the challenge of sensor array optimization, as illustrated in Fig. 1. The methodology we employ involves the following steps:

- Select explainable model algorithms that allow for the extraction of feature importance.
- Utilize the collected sensing data to train all chosen models and subsequently extract the importance of various features.
- Validate and benchmark the models to identify the best-performing ones.
- Employ the selected models in a voting mechanism, weighted by their performance, to choose the most relevant sensors.
- Establish two operational modes for the sensor array: the 'Green mode' and the 'Blue mode' to fulfill different sensing requirements.

## 3. Results and Discussion

### 3.1. Ensemble Learning Setup

Fig. 1 outlines the workflow for implementing our dual-mode CRS array strategy, utilizing a dataset derived from groundwater CRS data. Details on sensor configurations and data

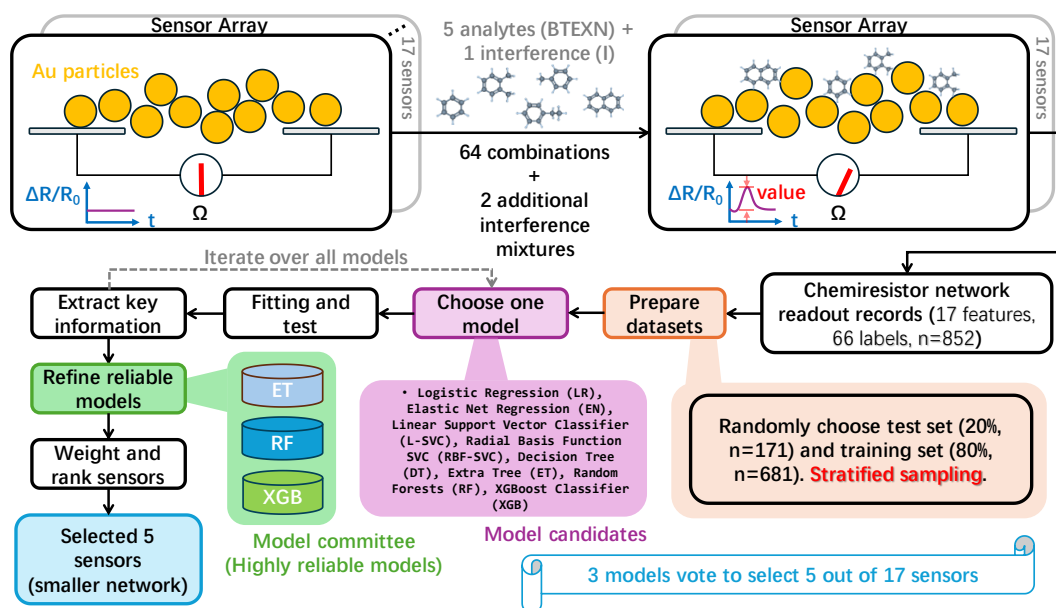


Fig. 1. The workflow of implementing the proposed strategy for the CRS array data. The details of the dataset and the fabricated sensors can be found in Supplementary Materials.

Analyte	Label	Concentration Range	Distribution
Benzene	B	44 - 120 $\mu\text{g L}^{-1}$	
Toluene	T	44 - 110 $\mu\text{g L}^{-1}$	
Ethylbenzene	E	44 - 120 $\mu\text{g L}^{-1}$	
p-Xylene	X	44 - 110 $\mu\text{g L}^{-1}$	
Naphthalene	N	44 - 160 $\mu\text{g L}^{-1}$	
Interferent	I	62 - 113 $\mu\text{g L}^{-1}$	

Table 1. The analytes' ingredients, concentrations, and distributions.

acquisition methodologies are elaborated in our prior publication [11]. In the present study, we employ a dataset comprising readout records from 17 sensors, each responding to 66 distinct analytes, either individual chemicals or chemical mixtures. This dataset encompasses 853 entries, where each entry features 17 sensor readings and a single label identifying the detected analyte. The modeling task is a supervised learning task that aims to train classification models to identify the labels of the CRS array's readout. Comprehensive information on the analytes, including their composition, concentrations, and distribution, is available in Table 1.

For each training and validation cycle, the dataset is partitioned into a training set (comprising 80% of the original experimental data) and a test set (accounting for the remaining 20%). Stratified sampling ensures that both subsets are representative, containing all unique labels. One round of training and validating models and extracting all important features costs only 8.9 seconds.

We then employ eight interpretable machine learning models, deliberately excluding deep

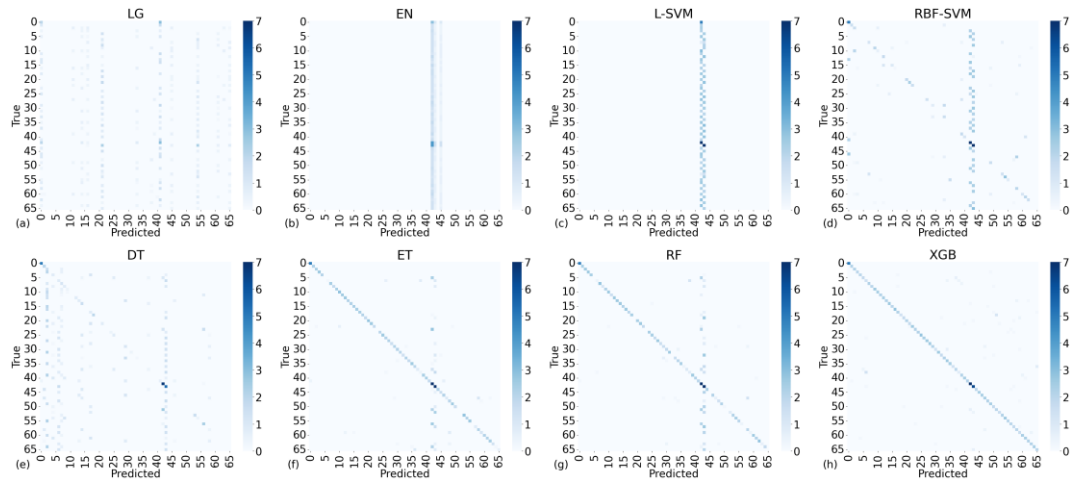


Fig. 2. The confusion matrices of the model candidates in the validation. The values in diagonal indicate the level of correct classification (the level of correct classification of the  $i$ -th analyte is represented by the value at the  $i$ -th row and column). (a) LG, (b) EN, and (c) L-SVM models cannot complete the classification task; (d) RBF-SVM and (e) DT can partially extract the patterns and perform the classification; while (f) ET, (g) RF, and (h) XGB perform well in the classification.

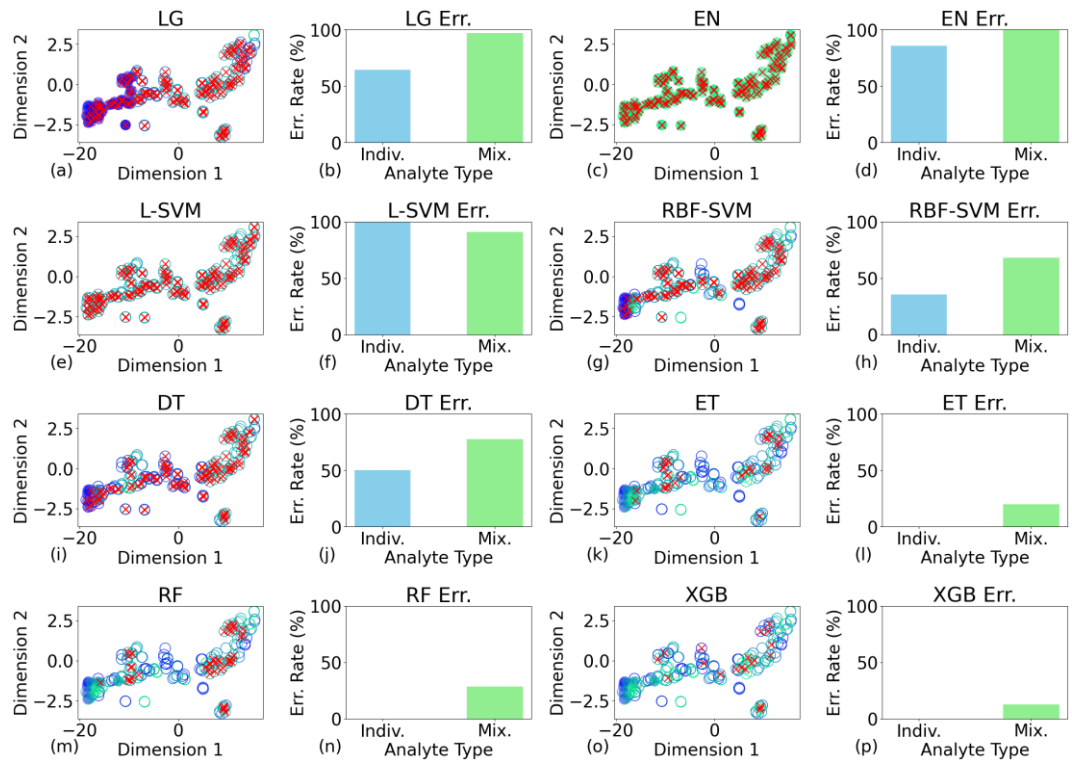


Fig. 3. First column, (a)-(m), and third column, (c)-(o), the 2D mapping of the data points in one validation shot by tSNE algorithm. Circles with different colors represent different test data, and those with the red error marks are incorrectly classified data points. Second column, (b)-(n), and fourth column, (d)-(p), the corresponding error rates in the classification. These results indicate that ET, RF, XGB are excellent candidates for serving the model committee.

neural network algorithms, to facilitate rapid and transparent predictive modeling. The

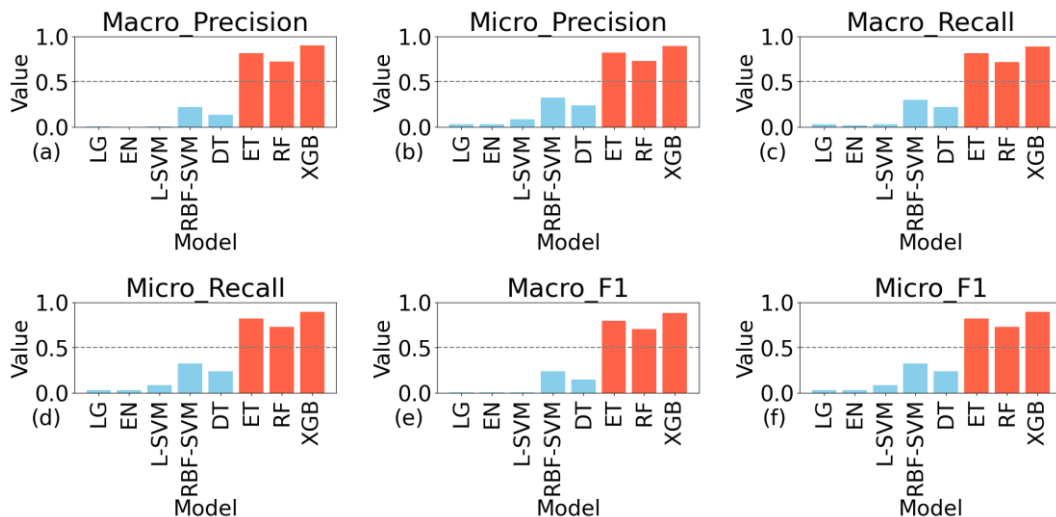


Fig. 4. The evaluation scores of the classification models. (a)-(f) denote the macro and micro scores, including the precision, recall, and F1, respectively. Only the ET, RF, XGB models (scores highlighted in red) can yield good classifications. Therefore, the ET, RF, and XGB are chosen as the members of the model committee for sensor selection.

selected models include Logistic Regression (LR), Elastic Net Regression (EN), Linear Support Vector Classifier (L-SVC), Radial Basis Function SVC (RBF-SVC), Decision Tree (DT), Extra Tree (ET), Random Forests (RF), and XGBoost Tree Classifier (XGB). Each model is trained using the training set and subsequently validated against the test set. Evaluation metrics are extracted post-validation, and the entire procedure is detailed in Fig. 1. Detailed information of the models can be found in Supplementary Material.

### 3.2. Model Committee

To construct the model ensemble, we rigorously evaluated the performance of each candidate model. Fig. 2 presents the confusion matrices for all eight models, revealing distinct variations in their classification capabilities. Specifically, the ET, RF, and XGB models demonstrate robust performance. In contrast, LG, EN, and L-SVC exhibit limited efficacy in data modeling post-training. The RBF-SVC and DT models achieve moderate success, as evidenced by the prominence of diagonal elements in their respective confusion matrices.

This performance assessment is further corroborated by a two-dimensional (2D) visualization of classification results (tSNE mapping), depicted in Fig. 3. The figure illustrates both the classification outcomes and the corresponding error rates for a single validation run. Red cross markers highlight misclassified data points, providing an intuitive gauge of each model's effectiveness. Notably, the ET, RF, and XGB models excel in classifying individual analytes, with only minor errors observed in the classification of mixed analytes.

A more objective and comprehensive evaluation is achieved through scoring the candidate models, as depicted in Fig. 4. Consistent with the observations from Figs. 2 and 3, ET, RF, and XGB emerge as the top-performing models, each achieving scores above 0.7 across all

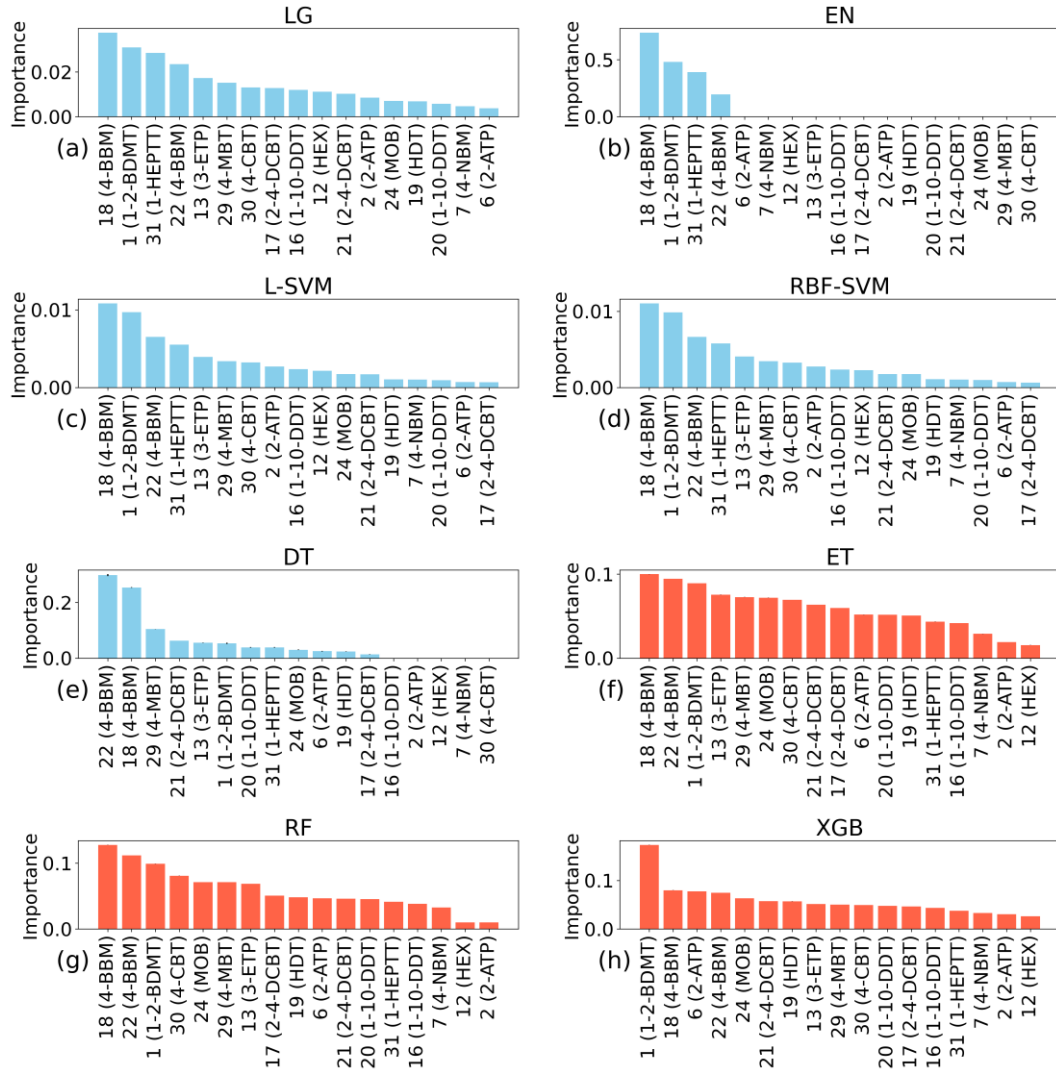


Fig. 5. The importance ranking of all sensors in the array, listed by eight models.

Although other models can extract an importance list (a)-(e), their results were abandoned due to low model performance scores; while the model committee's, (f) ET, (g) RF, and (h) XGB's, results were taken into account because of high performance in modeling.

metrics. Notably, XGB excels with scores exceeding 0.88, affirming its robust modeling capabilities. In contrast, the remaining models fall short, registering significantly lower scores and thereby disqualifying themselves from inclusion in the model ensemble. Consequently, the ensemble should comprise ET, RF, and XGB.

### 3.3. Sensor Array Optimization

Fig. 5 presents the sensor importance rankings for classification across all models. It's crucial to note that these rankings assess the role of sensor readouts in the classification process, rather than their sensitivities or energy consumption. We focus on the top three best-performing models, highlighted in red, for a more reliable interpretation of sensor importance. Interestingly, the sequence of sensor importance varies among these models, such as ET, RF,

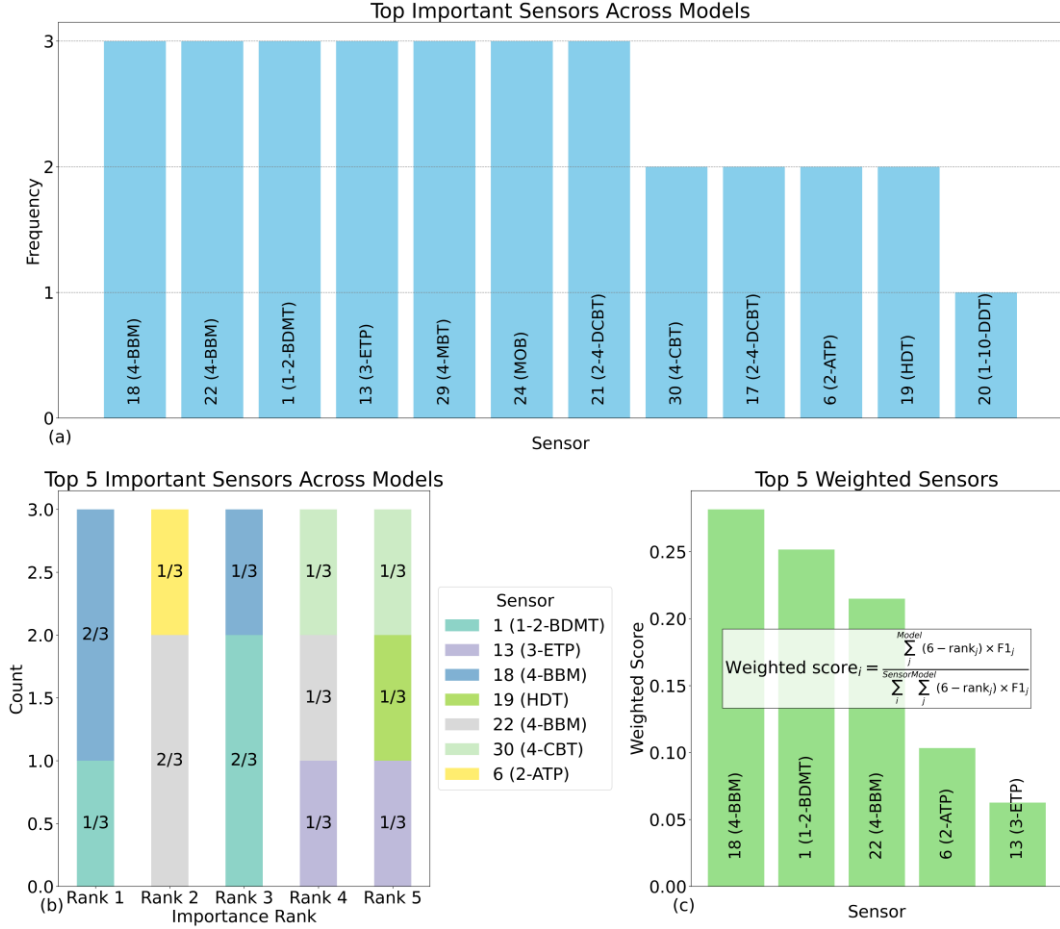


Fig. 6. The statistics of the sensor selection by the model committee: (a) the frequency, (b) the counts of the ranks, and (c) the weighted scores of the elected sensors across models. Using frequency and ranking counts cannot conclude a straightforward sensor list, while the weighted scores can easily generate a list of selected sensors.

and XGB.

Relying solely on a single ML model to identify the most impactful sensors for accurate classification is not advisable. Even a straightforward frequency count of sensors appearing in the top 5 positions across each model's list falls short in pinpointing key performance indicators, as depicted in Fig. 6(a). A more robust solution is a voting mechanism within the model committee, illustrated in Fig. 6(b). However, performance disparities exist even among these committee members. Simply averaging their sensor rankings without accounting for these variations could dilute the accuracy of the final selection. To mitigate this, we use the models' F1 scores as weights to fine-tune the ultimate choice of sensors:

$$\text{Weighted score}_i = \frac{\sum_j^{\text{Model}} (6 - \text{rank}_i) \times F1_j}{\sum_i^{\text{Sensor}} \sum_j^{\text{Model}} (6 - \text{rank}_i) \times F1_j} \quad (9)$$

Consequently, the weighted score for the  $i$ -th sensor is calculated as its rank score  $(6 - \text{rank}_i)$  across all models, each weighted by the model's corresponding F1 score  $F1_j$ .

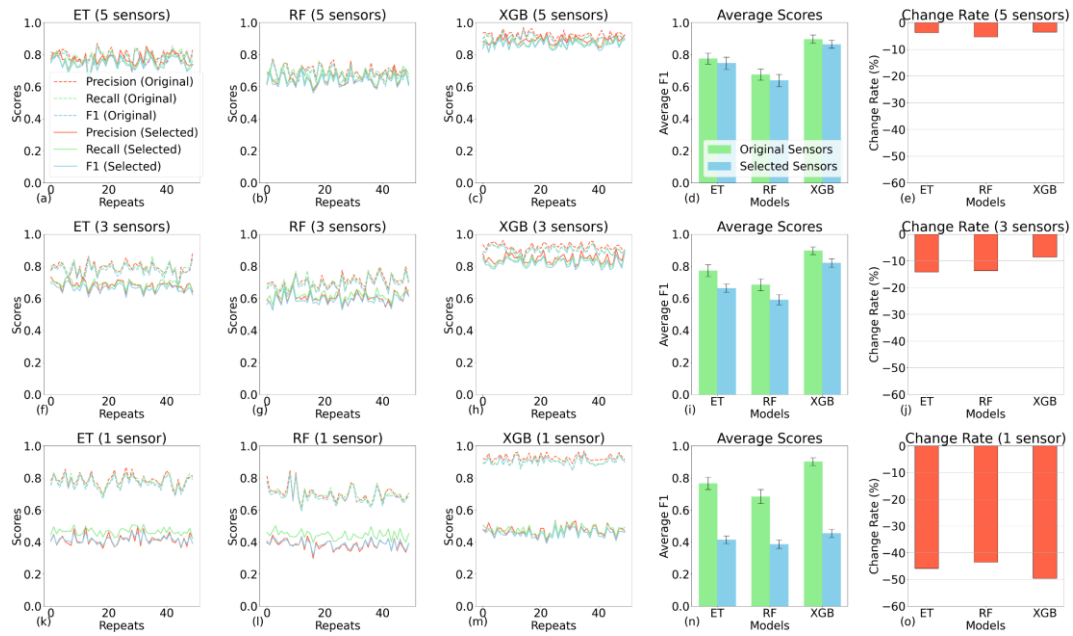


Fig. 7. The performance scores of the CRS array in different working modes. (a)-(c), (f)-(h), and (k)-(m) are the precision, recall, and F1 scores of the array working in different modes (with different sensors) in multiple validation repeats (each repeat will split the training set and validation set with stratified sampling randomly); (d), (i), and (n) are the average of the F1, with error bars showing the deviation; (e), (j), and (o) are the reduction in average F1 in different working modes (different numbers of activated sensors).

This sum is then normalized by dividing it by the total scores of all sensors across all models in the committee. Utilizing this weighted score, we can compile a list that ranks all sensors based on their impact on sensing, from highest to lowest, as depicted in Fig. 6(c) where we show top 5 critical sensors only.

Leveraging the list of the top 5 critical sensors, we introduce two operational modes for the CRS array: the Blue mode, where all sensors are active for maximum detection capability, and the Green mode, where only the top 5 key sensors are operational to conserve energy without significantly compromising detection capability. More drastically, we can opt to use only the top 3 most critical sensors for the Green mode, depending on the specific environmental conditions.

To evaluate the efficacy of the Green mode, we compare the detection capabilities of the CRS array working in both Blue and Green modes, as illustrated in Fig. 7. The first three subfigures in each row of Fig. 7 display the array's detection capabilities in varying configurations—using 5, 3, and 1 sensors. Notably, the Green mode with 5 sensors closely matches the Blue mode in detection capability. While fewer sensors result in diminished capability, the 3-sensor Green mode could be advantageous in scenarios where energy conservation is a critical constraint. For this assessment, we employ the validation set and model scores (precision, recall, and F1) as performance metrics.

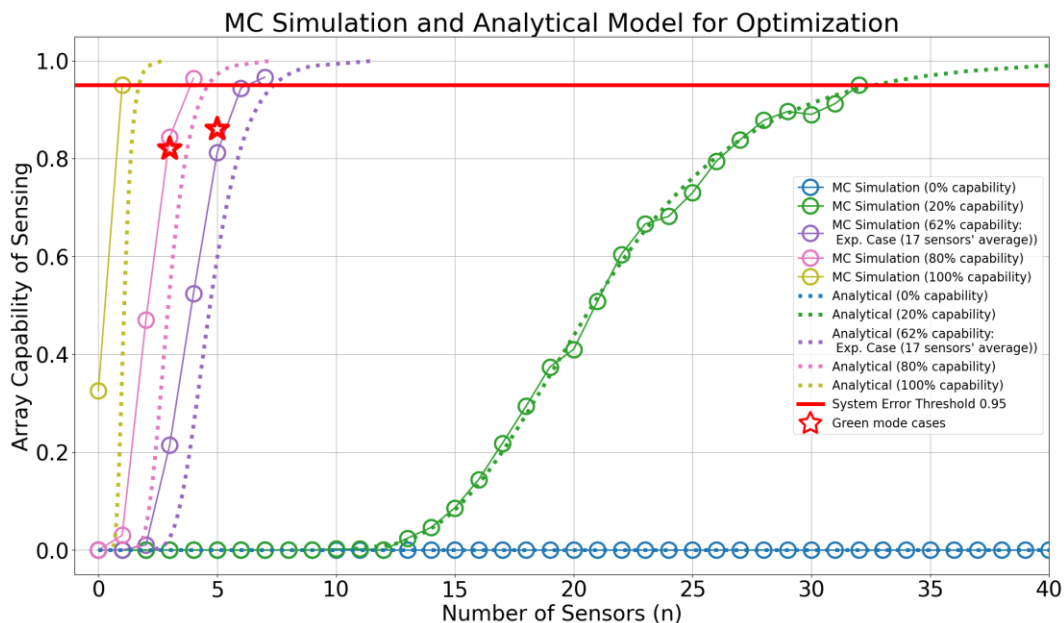


Fig. 8. The results of the Green modes benchmarking with the Monte Carlo simulation and the analytical modeling results. The Green mode achieved by the proposed strategy (red stars) can approach the theoretical limit of optimizing the CRS array. 100% capability's line offsets the vertical direction due to the variance of the Gaussian distribution in MC simulation.

Figs 7(d), (i), and (n) offer a direct comparison of F1 scores between the two modes. Utilizing the XGB model for readout, both the 5 and 3-sensor Green modes achieve F1 scores above 0.8, albeit with a slight decline compared to the Blue mode. A more detailed view of this F1 score reduction is presented in Figs 7(e), (j), and (o). Here, it's evident that the 5-sensor Green mode significantly reduces energy consumption—by as much as 70% if we assume uniform power budgets across sensors—while only causing a sub-5% drop in detection capability. In contrast, the 3-sensor Green mode sees a maximum capability reduction of 15% but offers an 82% cut in power consumption. Operating with just a single sensor, however, results in a low F1 score, indicating ineffective analyte identification.

### 3.4. Validation with Theory

The efficacy of our optimized strategy can be corroborated through both theoretical calculations and Monte Carlo (MC) simulations, as depicted in Fig. 8. In this figure, the analytical results closely align with the MC simulations, with an error margin of less than one sensor, serving as robust cross-validation. The red stars in the figure represent the outcomes achieved using our proposed Green modes. It's evident that a higher individual sensor capability within the CRS array allows for fewer sensors to achieve a given level of array sensing performance. In our experiments, the average capability across all sensors is 62%, denoted in dark grey. Utilizing our strategy, we've reduced the sensor count to 5 and 3 in the Green modes, surpassing the performance estimates from both MC simulations and

theoretical calculations (yellow dash line) based on a 62% capability. Remarkably, these numbers approach the theoretical limit, represented by the 100% capability line in light grey. Additionally, the selected sensors in the model committee's choices are all 100%-capability sensors, capable of identifying all analytes (see Supplementary Materials for details). This suggests that our strategy adeptly identifies the most effective sensors in the array and leverages their collective, non-linear working patterns to optimize readout. Consequently, the array's detection capability not only exceeds the average but also approaches the theoretical limit.

These findings affirm the promise of our weight-based voting strategy within the model committee for optimizing the CRS array. They also suggest that the energy-efficient Green mode achieved by the proposed strategy could be a stepping stone toward the development of low-cost, easily fabricated next-generation IoT sensors.

#### **4. Conclusion**

This study introduces an optimization strategy for Chemiresistive Sensor (CRS) arrays, leveraging a model committee approach to enhance both sensing simplicity and energy efficiency. Validated through theoretical analysis and Monte Carlo simulations, the strategy proves to be both effective and accurate. Specifically, we propose two working modes—Blue and Green—to achieve optimal detection capabilities and energy conservation, respectively.

Our strategy successfully identifies the most impactful sensors for accurate classification and optimizes sensor selection through a weighted voting mechanism within the model committee. This not only elevates the overall detection capability of the array but also significantly reduces energy consumption. In particular, the Green mode allows for comparable detection capabilities to the Blue mode while operating with only 5 or 3 key sensors, thereby substantially reducing energy expenditure. Furthermore, our approach demonstrates adaptability and scalability, capable of automatically selecting the best sensors within the array and extracting their nonlinear working patterns for optimized readout. This not only enhances the detection capability of the array but also brings it closer to theoretical limits.

In summary, this study presents an effective optimization method for CRS arrays, promising significant implications for the development of low-cost, easily fabricable next-generation IoT sensor terminals.

#### **5. Experimental Section**

The experimental data for this paper was collected from experiments presented in previous works [10], [11]. Briefly, sensors consisted of gold nanoparticle films spread across interdigitated electrodes. The gold nanoparticles of different sensors were functionalized with different thiols that are listed in ref [10]. The thiols defined the partial selectivity with which different sensors would interact with different analytes, i.e. the 1,10-decanedithiol

functionalized sensor (1-10-DDT) had a relatively weak response to naphthalene in comparison to the 1-heptanethiol functionalized sensor (1-HEPTT).

The sensor array was exposed to mixtures of benzene (B), toluene (T), ethylbenzene (E) p-xylene (X), naphthalene (N), and Interferants (I) a “BTEX free” mixture of organics that could potentially interfere with the sensor array’s response to B, T, E, X, or N. A full factorial Design of Experiment (DOE) was performed with every possible combination of B, T, E, X, N, I prepared and exposed to the sensor array. Each mixture was exposed to the sensor array 12 times with response (maximum relative resistance change) of every sensor in the array recorded each time. In total the dataset contains 66 different mixtures with an occasional repeat giving a total of 71 samples, each exposed 12 times (852 rows) with the concentration of each component (6 columns) and the responses of 17 sensors (17 columns). The original dataset is freely available in the supplementary material of [11].

## 6. Acknowledgement

This work was partially supported by CSIRO Impossible-Without-You program.

## 7. References

- [1] A. V. Agrawal, N. Kumar, and M. Kumar, “Strategy and Future Prospects to Develop Room-Temperature-Recoverable NO<sub>2</sub> Gas Sensor Based on Two-Dimensional Molybdenum Disulfide,” *Nano-Micro Lett.*, vol. 13, no. 1, p. 38, Jan. 2021, doi: 10.1007/s40820-020-00558-3.
- [2] M. Hartwig, R. Zichner, and Y. Joseph, “Inkjet-Printed Wireless Chemiresistive Sensors—A Review,” *Chemosensors*, vol. 6, no. 4, Art. no. 4, Dec. 2018, doi: 10.3390/chemosensors6040066.
- [3] K. Lim *et al.*, “A Transparent Nanopatterned Chemiresistor: Visible-Light Plasmonic Sensor for Trace-Level NO<sub>2</sub> Detection at Room Temperature,” *Small*, vol. 17, no. 20, p. 2100438, 2021, doi: 10.1002/sml.202100438.
- [4] W.-C. Chen *et al.*, “Study of a Palladium (Pd)/Aluminum-Doped Zinc Oxide (AZO) Hydrogen Sensor and the Kalman Algorithm for Internet-of-Things (IoT) Application,” *IEEE Trans. Electron Devices*, vol. 67, no. 10, pp. 4405–4412, Oct. 2020, doi: 10.1109/TED.2020.3018084.
- [5] H. Schlicke, S. C. Bittinger, H. Noei, and T. Vossmeier, “Gold Nanoparticle-Based Chemiresistors: Recognition of Volatile Organic Compounds Using Tunable Response Kinetics,” *ACS Appl. Nano Mater.*, vol. 4, no. 10, pp. 10399–10408, Oct. 2021, doi: 10.1021/acsnm.1c01892.
- [6] V. Montes-García, M. A. Squillaci, M. Diez-Castellnou, Q. K. Ong, F. Stellacci, and P. Samorì, “Chemical sensing with Au and Ag nanoparticles,” *Chem. Soc. Rev.*, vol. 50, no. 2, pp. 1269–1304, Feb. 2021, doi: 10.1039/D0CS01112F.
- [7] B. Szulczyński and J. Gębicki, “Currently Commercially Available Chemical Sensors Employed for Detection of Volatile Organic Compounds in Outdoor and Indoor Air,” *Environments*, vol. 4, no. 1, Art. no. 1, Mar. 2017, doi: 10.3390/environments4010021.

- [8] Y. Milyutin *et al.*, "Fabricating and printing chemiresistors based on monolayer-capped metal nanoparticles," *Nat. Protoc.*, vol. 16, no. 6, Art. no. 6, Jun. 2021, doi: 10.1038/s41596-021-00528-y.
- [9] L. Spinelle, M. Gerboles, G. Kok, S. Persijn, and T. Sauerwald, "Review of Portable and Low-Cost Sensors for the Ambient Air Monitoring of Benzene and Other Volatile Organic Compounds," *Sensors*, vol. 17, no. 7, Art. no. 7, Jul. 2017, doi: 10.3390/s17071520.
- [10] J. S. Cooper *et al.*, "Detecting and discriminating pyrethroids with chemiresistor sensors," *Environ. Chem.*, vol. 16, no. 7, pp. 553–559, Aug. 2019, doi: 10.1071/EN19133.
- [11] J. S. Cooper *et al.*, "Quantifying BTEX in aqueous solutions with potentially interfering hydrocarbons using a partially selective sensor array," *Analyst*, vol. 140, no. 9, pp. 3233–3238, Apr. 2015, doi: 10.1039/C5AN00223K.
- [12] M. Khatib and H. Haick, "Sensors for Volatile Organic Compounds," *ACS Nano*, vol. 16, no. 5, pp. 7080–7115, May 2022, doi: 10.1021/acsnano.1c10827.
- [13] R. A. Potyrailo, "Toward high value sensing: monolayer-protected metal nanoparticles in multivariable gas and vapor sensors," *Chem. Soc. Rev.*, vol. 46, no. 17, pp. 5311–5346, Aug. 2017, doi: 10.1039/C7CS00007C.
- [14] F. J. Ibañez and F. P. Zamborini, "Chemiresistive Sensing with Chemically Modified Metal and Alloy Nanoparticles," *Small*, vol. 8, no. 2, pp. 174–202, 2012, doi: 10.1002/smll.201002232.
- [15] G. Konvalina and H. Haick, "Sensors for Breath Testing: From Nanomaterials to Comprehensive Disease Detection," *Acc. Chem. Res.*, vol. 47, no. 1, pp. 66–76, Jan. 2014, doi: 10.1021/ar400070m.
- [16] N. Bachar, L. Liberman, F. Muallem, X. Feng, K. Müllen, and H. Haick, "Sensor Arrays Based on Polycyclic Aromatic Hydrocarbons: Chemiresistors versus Quartz-Crystal Microbalance," *ACS Appl. Mater. Interfaces*, vol. 5, no. 22, pp. 11641–11653, Nov. 2013, doi: 10.1021/am403067t.
- [17] M. G. Campbell, S. F. Liu, T. M. Swager, and M. Dincă, "Chemiresistive Sensor Arrays from Conductive 2D Metal–Organic Frameworks," *J. Am. Chem. Soc.*, vol. 137, no. 43, pp. 13780–13783, Nov. 2015, doi: 10.1021/jacs.5b09600.
- [18] R. J. Rath, S. Farajikhah, F. Oveissi, F. Dehghani, and S. Naficy, "Chemiresistive Sensor Arrays for Gas/Volatile Organic Compounds Monitoring: A Review," *Adv. Eng. Mater.*, vol. 25, no. 3, p. 2200830, 2023, doi: 10.1002/adem.202200830.
- [19] Z. Xu, X. Shi, and S. Lu, "Integrated sensor array optimization with statistical evaluation," *Sens. Actuators B Chem.*, vol. 149, no. 1, pp. 239–244, Aug. 2010, doi: 10.1016/j.snb.2010.05.038.
- [20] R. Polikar, R. Shinar, L. Udpa, and M. D. Porter, "Artificial intelligence methods for selection of an optimized sensor array for identification of volatile organic compounds," *Sens. Actuators B Chem.*, vol. 80, no. 3, pp. 243–254, Dec. 2001, doi: 10.1016/S0925-4005(01)00903-0.
- [21] J. W. Gardner, P. Boilot, and E. L. Hines, "Enhancing electronic nose performance by sensor selection using a new integer-based genetic algorithm approach," *Sens. Actuators B Chem.*, vol. 106, no. 1, pp. 114–121, Apr. 2005, doi: 10.1016/j.snb.2004.05.043.
- [22] D. Gómez and A. Rojas, "An Empirical Overview of the No Free Lunch Theorem and Its Effect on Real-World Machine Learning Classification," *Neural Comput.*, vol. 28, no. 1, pp.

- 216–228, Jan. 2016, doi: 10.1162/NECO\_a\_00793.
- [23] D. H. Wolpert and W. G. Macready, “No free lunch theorems for optimization,” *IEEE Trans. Evol. Comput.*, vol. 1, no. 1, pp. 67–82, Apr. 1997, doi: 10.1109/4235.585893.
- [24] T. Itoh *et al.*, “Discrimination of volatile organic compounds using a sensor array via a rapid method based on linear discriminant analysis,” *Sens. Actuators B Chem.*, vol. 387, p. 133803, Jul. 2023, doi: 10.1016/j.snb.2023.133803.
- [25] M. A. H. Khan, B. Thomson, R. Debnath, A. Motayed, and M. V. Rao, “Nanowire-Based Sensor Array for Detection of Cross-Sensitive Gases Using PCA and Machine Learning Algorithms,” *IEEE Sens. J.*, vol. 20, no. 11, pp. 6020–6028, Jun. 2020, doi: 10.1109/JSEN.2020.2972542.
- [26] H. Hu, M. Kantardzic, and T. S. Sethi, “No Free Lunch Theorem for concept drift detection in streaming data classification: A review,” *WIREs Data Min. Knowl. Discov.*, vol. 10, no. 2, p. e1327, 2020, doi: 10.1002/widm.1327.
- [27] K.-L. Du and M. N. S. Swamy, “Combining Multiple Learners: Data Fusion and Ensemble Learning,” in *Neural Networks and Statistical Learning*, K.-L. Du and M. N. S. Swamy, Eds., London: Springer, 2019, pp. 737–767. doi: 10.1007/978-1-4471-7452-3\_25.